Molecular Simulation, 1999, Vol. 22, pp. 57–80
Reprints available directly from the publisher
Photocopying permitted by license only

DATA COLLECTION FOR THE CALCULATION OF PHASE EQUILIBRIA

L. A. CORNISH[a,*] and M. J. WITCOMB[b]

[a] *School of Process and Materials Engineering, University of the Witwatersrand, Private Bag 3, WITS, 2050, South Africa;*
[b] *Electron Microscope Unit, University of the Witwatersrand, Private Bag 3, WITS, 2050, South Africa*

(Received October 1998; accepted November 1998)

Data collection for the calculation of phase equilibria is discussed, with reference to the Al–Ni–Re system. Since there were conflicting data for the Al–Re system and no data at all for the ternary system, an extensive experimental programme was initiated using SEM with EDS, and XRD. X-ray data were modelled for the likely structures of some phases.

Experimental results indicated that a previously unreported binary eutectic reaction forming Al_2Re_3 and Al_3Re was found at ~34 at.% Re. With the exception of $Al_{12}Re$ (which was only found as a minor, finely divided component), all intermetallic phases were demonstrated to have a composition range between 1.5 and ~5 at.%.

In the Al–Ni–Re ternary system, (Re) had the greatest solubility. The Al_3Re and Al_6Re phases extended within the ternary to ~6 at.% Ni, whereas AlNi and $AlRe_2$ showed ~3 at.% extension. The remaining phases had very much lower solubility limits. The liquidus surface was derived from the sequence of solidification. Since these findings were largely deduced from metallographic studies, problems associated with the interpretation of microstructures were discussed in general terms.

Keywords: Data collection; phase equilibria; Al–Re; Al–Ni–Re

INTRODUCTION

A typical metallurgical phase equilibrium diagram indicates the phases which are stable at different temperatures and compositions. Thus, the phase diagram is an expression derived from the comparison of Gibbs free energy data from different phases. There are two main methods of deriving phase equilibria. The first is by experimentation. This can take time,

*Corresponding author.

can be very expensive, and a degree of expertise is required. A more modern approach is to utilise stored data, usually thermodynamic, to calculate the phase diagram. This approach is favourable when there is a reasonable amount of good consistent data. The main advantage of the latter approach is that the data can be assessed for consistency, and applied in the calculation of higher order phase diagrams, for example, to calculate ternary phase diagrams from binary equilibria. Obviously, any ternary data is helpful, and the component binary systems must be well documented. However, the calculation of phase equilibria from thermodynamic data has disadvantages: good quality data must be available, and there must be a reliable way of expressing the data. When these conditions cannot be met, it is impossible to reliably and accurately obtain a good computer calculation.

THERMODYNAMIC BACKGROUND

The state of equilibrium implies that the system must be at the lowest energy at the specified conditions, and most calculations use minimisation optimisation techniques. Additionally, when more than one phase is in equilibrium, this becomes a constrained optimisation. The Gibbs free energy has to be minimised subject to the constraints that the total amount of each element must remain constant for all elements, and also that the sum of all the elements must be constant. Typically, Lagrange's undetermined multipliers, or a Newton-Raphson method, is utilised to find the minimum energy, and then the phase compositions at this energy.

There are also certain "rules" which are derived from thermodynamic principles, but which can also be assessed by the shape of the phase diagram. These include: phase boundaries must divide regions with one phase difference; all lines must be smooth; and adherence to the phase rule [1].

The overall shapes of the Gibbs free energy curves are dependent on the type of phase, and the depth of the parabola is defined by the difference in the Gibbs free energy of mixing between the components (ΔG_{mix}). Thus a substitutional solid solution, especially where the atoms are of similar size, has a wide, shallow parabola, whereas an intermetallic compound with little or no flexibility in its packing (and hence limited compositional stability), has a very steep and narrow parabola. However, the overall optimisation of the Gibbs free energy curves may mean that the lowest overall Gibbs free energy is attained at slightly off-stoichiometric compositions for the intermetallic phases, especially for two- or three-phase regions.

The easiest phase diagrams to derive are binary equilibria, because good data are usually readily available. However, another important aspect which must be considered is the bonding between the individual atoms. If there is no favoured bonding, *i.e.*, the choice is totally random, then the enthalpy of mixing is zero ($\Delta H_{mix} = 0$), and the system is said to be ideal in behaviour. However, even in solid solutions, and especially in compounds, this is unlikely to be true, and certain specie bonds will be more favoured. This leads to a non-zero ΔH_{mix} term, and an excess Gibbs free energy term which contains interaction parameters to describe the interactions for the given species. A number of models have been derived to express the interaction parameters [2], and these depend on the type of bonding, for example, the regular solution, and the sub-regular solution. Thus, once there is a deviation from ideality, interaction parameters are necessary. Expressions are needed for each combination of non-similar atoms: for example, in a ternary system a-b-c (where a, b and c are elements or compounds – as in many ceramic phase diagrams): interaction parameters would be necessary for ab, ac, bc and abc combinations. Often there are no data for the ternary interaction parameter (abc), although a number of formalisms can be chosen to approximate this parameter from binary data [2–6]. Occasionally, the true ternary interaction parameter is small, and, as a result, there is little difference between the predicted phase diagram calculated without it and that obtained from experimental data [7].

DATA ACQUISITION FOR PHASE EQUILIBRIA STUDIES

There is a very wide range of published data available, and there is a definite hierarchy of the usefulness of the different types of data. Although all data are useful and can be applied in the calculation of phase equilibria, the hierarchy is defined by how well the data has been assessed to be both self-consistent and consistent with other work. As one moves down the hierarchy, the data will have been less well assessed, and so the possibility of being less accurate increases.

The most reliable data are those which have already been utilised for phase equilibria studies or have been assessed in another way, for example, in the Lukas program [8]. The second broad category is published lattice parameters (or any other thermodynamic shorthand which would allow the easy derivation of the Gibbs free energy values). The third most desirable data type are published values of thermodynamic data, such as JANAF Tables [9], or Hultgren [10]. These data are usually from different experimental

sources, and have been collected and compared over relevant temperature ranges. Next on the list are published experimental data. These include any data which can be found in the literature, and whilst such data are most likely to have been peer-reviewed, sometimes there is little other reported data for a rigorous in-depth comparison. The least desirable type for phase equilibria calculations are raw experimental data. Usually this type of data is a last resort, and it is only employed if there are no other inputs. The great weakness is that there is nothing to compare these data against, and depending on the researcher, the errors might not have been rigorously assessed. On the other hand, when the same researcher is actually collecting the data for a specific assessment and subsequent use, then that researcher is probably most likely to be able to collate and assess the results most effectively, being aware of the relative accuracies of the different techniques employed. The integrity of the data increases as more different and complementary techniques are employed.

EXAMPLES OF EXPERIMENTAL TECHNIQUES FOR THE ACQUISITION OF PHASE DIAGRAM RAW DATA

Although there are numerous experimental techniques, the ones discussed below are those recommended by the authors because they are reasonably readily available in most laboratories, and are fairly straightforward to utilise. They are probably the most common techniques, and are also used by workers in other disciplines.

For phase diagram work, as-solidified samples are usually recommended, especially for an investigation of the liquid reactions, including the liquidus surface. Samples which have experienced direct solidification are useful because they are more likely to show most, if not all, of the phases which are possible, including those which are not stable at lower temperatures. Depending on the constraints of the particular system, for example, melting points, volatility and reactiveness, the samples can be melted in a normal furnace, or in an arc-melted button furnace. The latter is especially useful when some of the aforementioned-constraints apply. Although sometimes diffusion couples have been employed, these are not recommended for systems other than binaries, because diffusion occurs between the different regions of the couples such that an iso-activity line is reached, and only then does diffusion occur to lower the Gibbs free energy of the system. Thus, if the system is interrupted before diffusion is completed, *i.e.*, before equilibrium has been attained, an erroneous equilibrium situation might be interpreted. The

advantage of using as-solidified samples over any other technique, such as powder metallurgy routes, is that the sequence of solidification events can be derived.

All samples, no matter how they were manufactured, can be annealed and quenched to derive the phase compositions at the annealing temperatures. These data can be used to compile an isothermal section, if there are sufficient samples. With solidified samples, one knows that any annealing will bring the sample closer to the equilibrium microstructure, even if by a small amount, but for powder metallurgy and diffusion couples, this might not necessarily be the case, as discussed above.

One of the most unappreciated techniques, especially outside the field of metallurgy, is metallography. By studying and being able to recognise the sequence of phases, one can deduce the phases and their mode of formation. Optical microscopy is often just used for a rapid perusal of microstructures in a new system, while scanning electron microscopy (SEM) is employed for more detailed analysis. SEMs can be used to give the relative average atomic numbers of the constituent phases, and the actual compositions can be analysed typically using Energy Dispersive Spectroscopy (EDS) on an SEM, or EDS and/or by Wavelength Dispersive Spectroscopy (WDS) on an electron microprobe. When such collected data are compared, together with X-ray diffraction data, to identify or verify the phases, it is possible to complete a full analysis in a relatively short time. Occasionally, one (or more) of the phases is very fine, and is too small to be entirely contained within the X-ray excitation volume generated by the electron beam in the SEM. In this case, transmission electron microscopy (TEM) might be used as well, due to its much smaller electron beam size and smaller X-ray excitation volume diameter. Although much more information can be gleaned from a TEM study, for example: possibly more accurate phase compositions, structure types and lattice parameters (both from electron diffraction data), the greater difficulty of sample preparation is sometimes a deterrent.

A separate and very versatile technique to identify phases is X-ray diffraction. Additionally, the technique can be utilised to derive phase proportions, although the errors can be higher than in other techniques. There are many other applications, but as these are not directly relevant to phase diagram studies, they will not be considered here.

There are a host of thermodynamic techniques, of which the most common and most commercially available is one of the family of differential thermodynamic analysis (DTA). By measuring and comparing the heat contents of a container holding the sample against a similar empty one, the phase transformation reactions and their associated temperatures can be

derived. Also, heat capacity data for the different phases, and enthalpies of the reactions themselves can be derived. Older thermodynamic techniques include calorimetry, to obtain enthalpies and heat capacity data, and e.m.f. measurements, from which activities can be gleaned.

OVERVIEW OF THERMO-CALC

Thermo-Calc is a commercial package which can be used for many different calculations, including phase equilibria with different representations (for example, binary, ternary and multi-component composition-temperature diagrams, isothermal sections, liquidus surfaces), mass phase fraction-temperature plots and Scheil solidification simulations [11]. Within the Thermo-Calc environment, there are different modules which can be accessed to undertake the different tasks, for example: data input and selection, thermodynamic calculation, data processing for graphical output, and data assessment. The latter module is for the assessment and subsequent processing of raw data for use in higher order system calculations.

The Thermo-Calc system also has a selection of databases, which are as valuable as the program utilities. There are databases for elemental information, chemical substances, solutions, steels, semi-conductors, Fe-containing slags, aqueous substances, geochemical systems, and finally, for sulphides, nitrides and oxides. As well as the basic elemental information, the databases contain expressions to describe the variation of Gibbs free energy with temperature, pressure and constitution. All data have been rigorously assessed, and there is also a module which only accesses assessed binary phase diagrams. There are also separate commercial databases for nickel- and aluminium-based alloys. Finally, there is the ability to input one's own data, and, of course, to assess it. The latter is important because in order to be able to derive higher order phase equilibrium diagrams, it is necessary to have good data from the lower order systems.

Thermo-Calc operates by calculating thermodynamic variables and by applying the phase rule to derive the invariant equilibria. The user inputs enough conditions such that there are zero degrees of freedom in the phase rule:

$$P + F = C + 2$$

where:

P = number of phases
F = degrees of freedom
C = number of components.

Thermo-Calc then calculates the Gibbs free energy of the system, given the input conditions. This is then repeated for some, if not all, of the known invariant points, and the other, unknown, invariant reactions can be derived by using the information previously calculated. If the program cannot successfully converge on a minimum Gibbs free energy by iteration, then an error message is output. The user must then change some of the given conditions, usually by simplifying them, and submit the new conditions.

CASE STUDY: THE Al–Ni–Re SYSTEM

Previous Work

A study was initiated of the Al–Ni–Re system once it was realised that the ternary data were not available in the literature. As is usual, information on the component binary diagrams were sought from the literature. The Al–Ni system was well known, with five intermetallic phases, and was even available as an assessed system in Thermo-Calc, although without the low-temperature Al_3Ni_5 phase. The Ni–Re system was much simpler; comprising only a peritectic reaction L + (Re) → (Ni), but the data were very limited. The Al–Re system had very contradictory data, although there had been a number of investigations [12–19]. Intriguingly enough, although the 1987 compilation of Massalski had a compiled phase diagram [20], the 1990 compilation stated that the data were too contradictory for a phase diagram [21]. In the latter compilation [21], ten intermetallic phases were reported, two with the helpful names χ (chi) and Al_xRe_y, and the different interpretations were tabulated. However, searching the relevant literature revealed the compositions of these phases [13, 19]. Two main versions of the phase diagram were available: Savitskii's [13] earlier version with measured reaction temperatures, and Schuster's later and much more extensive version [19] (Fig. 1), which employed Savitskii's [13] temperatures. Additionally, X-ray work had been reported by several workers [13, 16, 19, 22–26], which suggested even more phases.

Problems with the Al–Re System

There are very good reasons why the Al–Re system had not been fully characterised, not least, the experimental difficulties. Firstly, there is a very large difference between the elemental melting points: 660°C for aluminium,

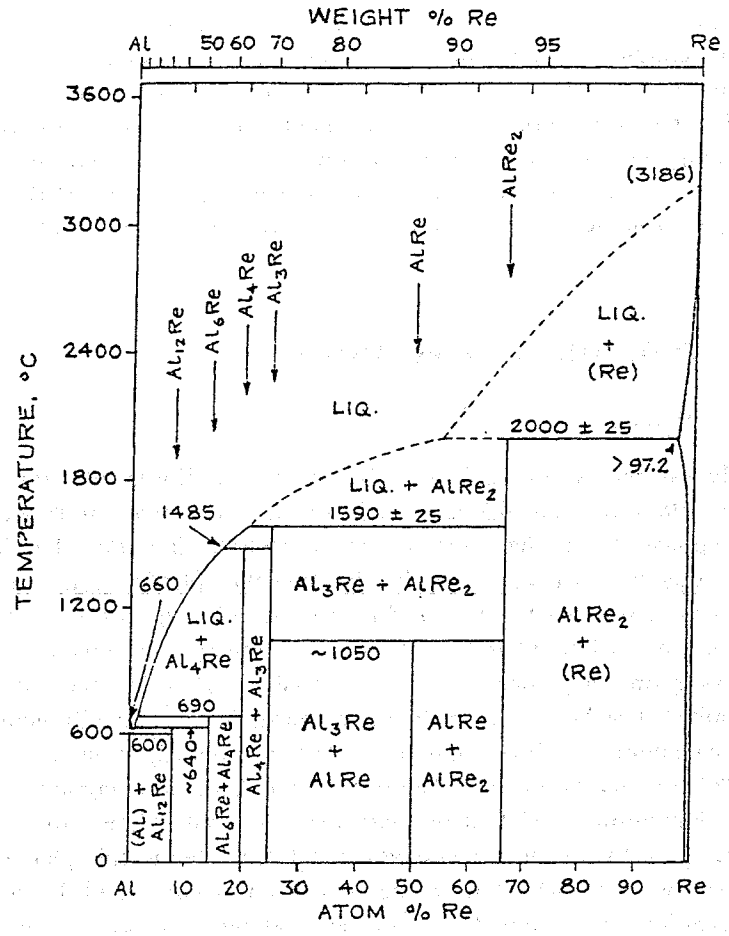

FIGURE 1 Al–Re phase diagram after Schuster [19].

and 3186°C for rhenium. This can lead to problems with specimen preparation, especially since aluminium has a high partial pressure. Thus, unless great care is taken, some of the aluminium is liable to vaporise, while the rhenium probably will not completely melt. Additionally, there are problems with identifying the phases, for two other non-related reasons. The first of these is that there is a sparsity of X-ray data, so that not all phases have been successfully characterised. The other difficulty is that there is a large difference in atomic number between the component elements: 13 for Al, and 75 for Re, as well as these elements being present in very different proportions in the different phases. Thus, the accuracy of EDS quantitative analyses could be compromised because of the magnitude of the X-ray

absorption of the heavy element on the light element, as well as the uncertainty in critical physical parameters such as: mass absorption coefficient and ionisation cross sections. Ideally, a number of different standards with accurately determined compositions spanning the phase diagram should be employed. However, this was not possible in the present study due to the nature of the phase diagram itself, and no single phase samples were obtained. However, in a similar phase diagram study of Al–Ir (atomic numbers 13 and 77 respectively) [27, 28] a near single-phase sample was obtained and analysed, then subjected to wet chemical analysis. The EDS analyses using the Ir L_α line for quantification yielding an Al composition of 75.7 ± 1.0 at.% Al showed better agreement, and was within experiment error, with the wet chemical analysis which gave a result of 76.5 ± 0.8 at.% Al, than when utilising the Ir M_α line, although the latter was larger, and had a better fit index.

Experimental Procedure

The samples were prepared as arc-melted buttons of ~ 2 g weight from chunks of the elements. Small samples were used because of the difficulty of melting all of the rhenium, and also because it was very time-consuming to cut rhenium into manageable small pieces. Samples were sectioned with a diamond blade, then prepared for metallographic examination. Since there was a wide range of hardnesses between the different phases, etching was unnecessary. Characterisation of the phases was undertaken at 20 kV using a SEM (JEOL JSM-840) and a LINK AN10000 EDS system. Metallography was used, particularly in deriving the sequence of the phases, by first identifying the primary solidified phase (from its characteristic structure: either dendritic or polygonal shape), and then deducing the formation order by working outwards from this phase, although the morphologies of the remaining phases were also taken into account. X-ray diffraction (XRD) was carried out using a SIEMENS D500 with molybdenum radiation, and a Philips PW1820 with copper radiation. Since there was a lack of data for some phases, the structures were obtained from the literature [21–26, 29], or estimated by reference to related compounds. These structures were then input to the CCMiller shareware program [30], and the peaks derived. Where the positions of the atoms were not known, different positions were tried. The experimental XRD spectra were compared with each other for phases known to be common (from EDS analyses and metallography), then with reported data [31], and finally, with the simulated data in a systematic fashion. In this way, the matches were ensured to be consistent.

RESULTS

Work was undertaken initially on the Al–Re binary system, and only after this had been better characterised, was an investigation of the ternary system attempted. Although some of the earlier high Re content binary samples had chunks of apparently unmelted Re, these were actually found to comprise three phases, confirming the complex nature of the phase diagram [32]. However, after a previously unreported eutectic had been found at ~34 at.% Re (Fig. 2) [33], samples of this (lower melting temperature) composition were made as master alloys for higher Re-content alloys, and the problem only reoccurred once.

The sequence of solidification could be easily derived from most of the microstructures; for example in Figure 3, the solidification sequence is the (ternary, *i.e.*, with all three elements present; here, some Ni) $AlRe_2$ dendrites, followed by the (ternary) Al_3Re plates, and finally the (ternary) Al_3Re + (ternary) AlNi eutectic. Peritectic reactions are easily identified, because the product surrounds the parent phase, and the interface between them is irregular since the outer regions of the parent phase are consumed.

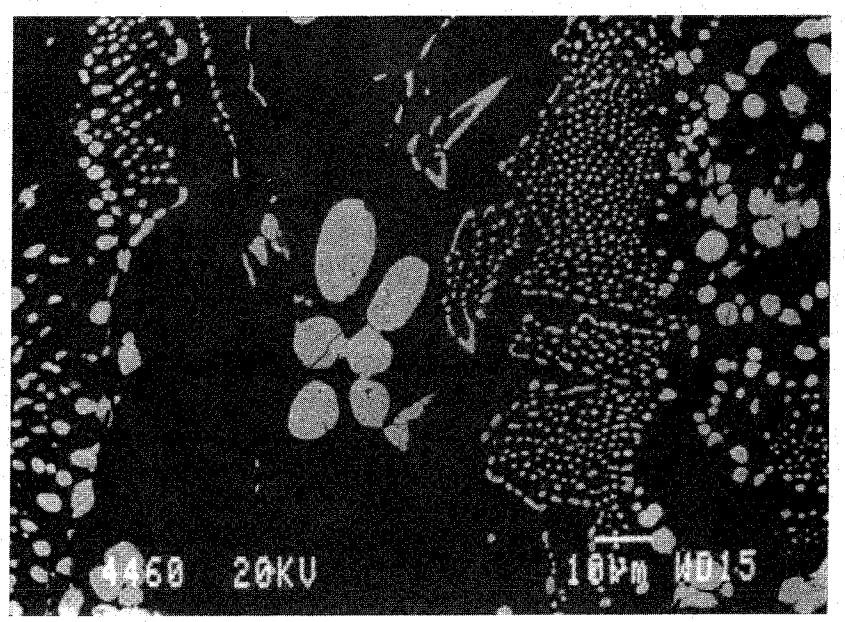

FIGURE 2 SEM image in backscattered electron mode. Al – 31 at.% Re alloy showing the previously unreported Al_3Re + Al_2Re_3 eutectic [33].

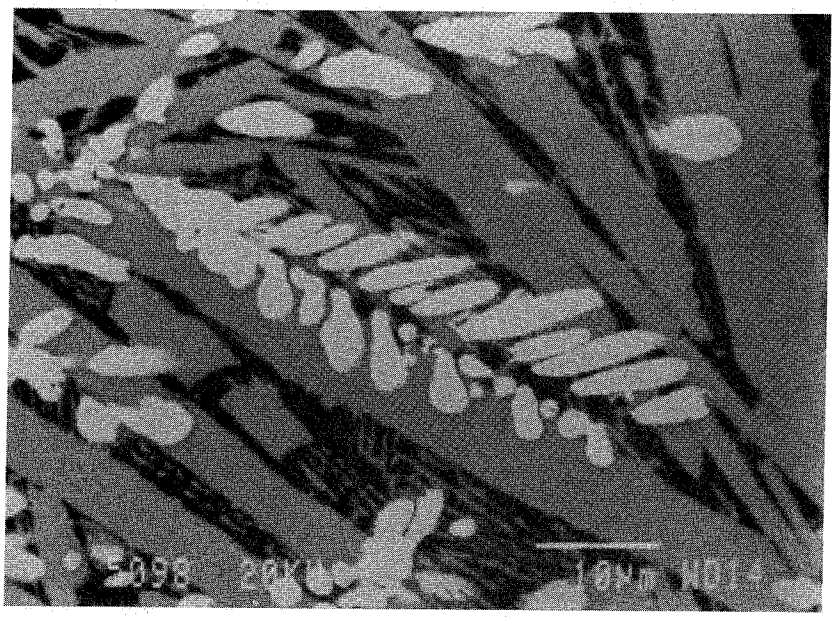

FIGURE 3 SEM image in backscattered electron mode. Al – 10 (at.%) Ni – 30 Re alloy: $AlRe_2$ dendrites (light), Al_3Re plates (grey) and Al_3Re + AlNi (dark) eutectic [33].

Some peritectic reaction examples include: $L + AlRe_2 \rightarrow Al_2Re_3$ (Fig. 4) [34], and $L + Al_4Re \rightarrow Al_6Re$ (Fig. 5) in the binary Al–Re system [32]. In the ternary Al–Ni–Re system, it was possible to discern some of the ternary invariant reactions directly, for example, L + (Re) → (ternary) AlNi + (ternary) Al_3Re (Fig. 6) [34]. However, in some instances it was not possible to discern the equilibrium reaction, because the microstructure showed obvious non-equilibrium changes. An example of this is shown in Figure 7, where there is a distinct boundary between two sets of solids [34]; this violates the phase rule and so cannot be an equilibrium microstructure.

The solidification compositions were plotted, together with the tie-lines from phases recognised (from the microstructures) to be in equilibrium with each other (Fig. 8). Although this is not an isothermal section, the diagram is nevertheless still useful, because if shows the approximate extents of all the phases. Utilising the information of the primary solidification phases with subsequent reactions, gleaned from the microstructures, a liquidus surface was produced (Fig. 9), which was consistent with all the samples.

The simulated XRD patterns were used to identify the remaining peaks after current experimental data had been compared with existing published data [34]. From such an exercise undertaken on all samples, the following

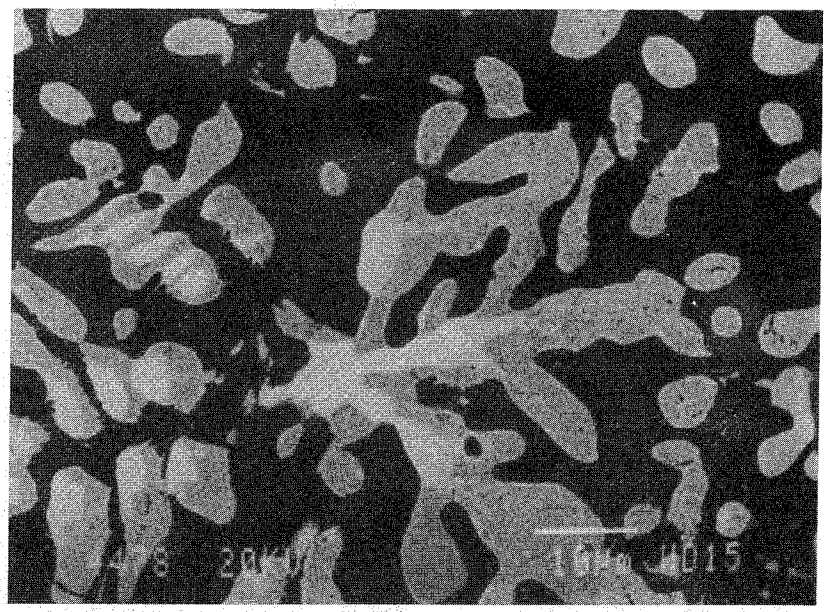

FIGURE 4 SEM image in backscattered electron mode. Al – 44 at.% Re alloy showing the L + $Al_2Re \rightarrow Al_2Re_3$ reaction: Al_2Re inner part of dendrites (light), Al_2Re_3 outer part of dendrites (grey) and Al_3Re matrix (dark) [34].

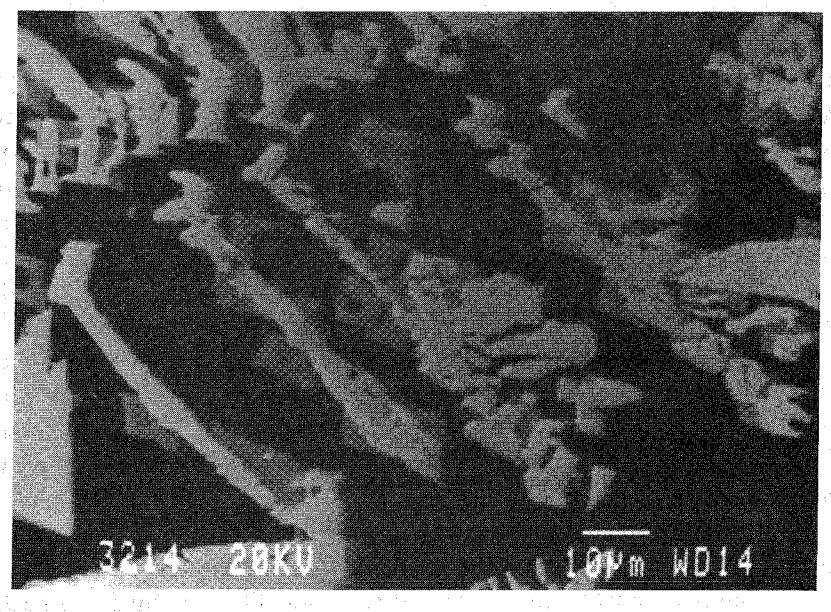

FIGURE 5 SEM image in backscattered electron mode. Al – 4 at.% Re alloy illustrating the L + $Al_4Re \rightarrow Al_6Re$ reaction: Al_4Re dendrites (light), Al_6Re faceted chunks (grey) and (Al) matrix (dark) [32].

FIGURE 6 SEM image in backscattered electron mode. Al – 15 (at.%) Ni – 5 Re alloy demonstrating the L + (Re) → Al_3Re + AlNi reaction: (Re) particles (light), and Al_3Re (grey) + AlNi (dark) eutectic [34].

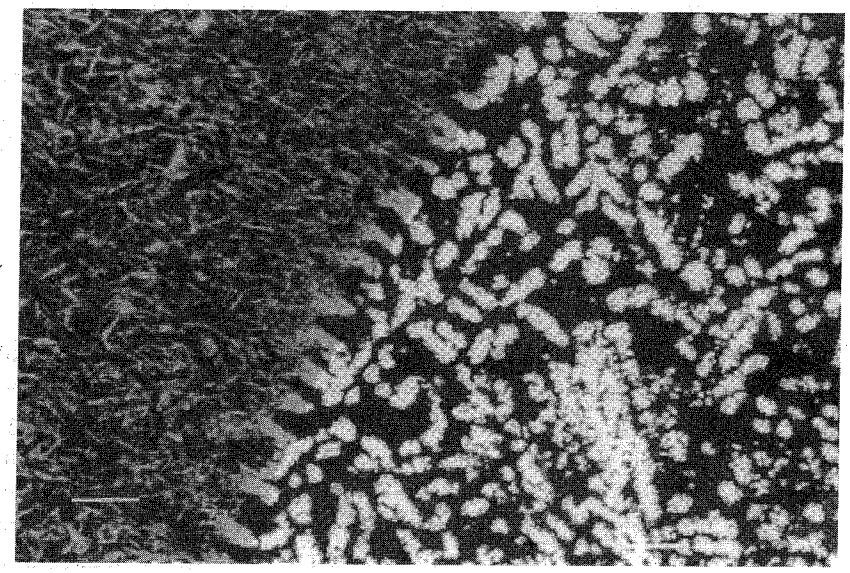

FIGURE 7 SEM image in backscattered electron mode. Al – 15 (at.%) Ni – 5 Re alloy showing a non-equilibrium boundary (too many phases are present) between two different regions. Coarse region: (Re) particles (light) with AlNi matrix (very dark); finer region: Al_3Re needles (light grey) and (Al) matrix (black) [34]. Bar represents 10 μm.

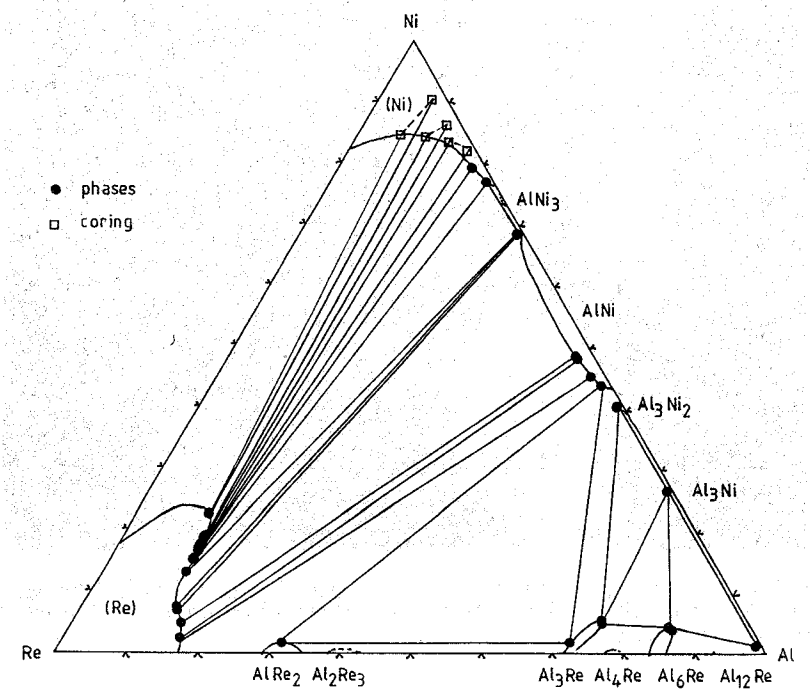

FIGURE 8 Solidification compositions in the Al–Ni–Re system (at.%).

structures were tentatively identified: Cu_7In_3 type for Al_4Re; Al_3Ni type for Al_3Re; and α-Mn type (cP20) for Al_2Re_3, with the Al atoms in the Mn_1 positions. However, more work is necessary on samples containing a much higher proportion of the phase in question to ascertain this.

INPUT FOR THERMO-CALC

The work so far has derived the solidification structures for a number of compositions spanning the Al–Ni–Re system. Since no annealing has been undertaken, the microstructures reflect the solidification compositions only. A plot has been produced of the ranges of solubility on solidification (Fig. 8), although it is likely that the solubilities will decrease with decreasing temperatures. Since the microstructures reflect the solidification sequence, the reactions can be identified, together with their reactants and product phases. From this information, the liquidus surface was determined. Work is in progress with differential thermal analysis (DTA) to determine the values of the specific reaction temperatures, which will be identified from

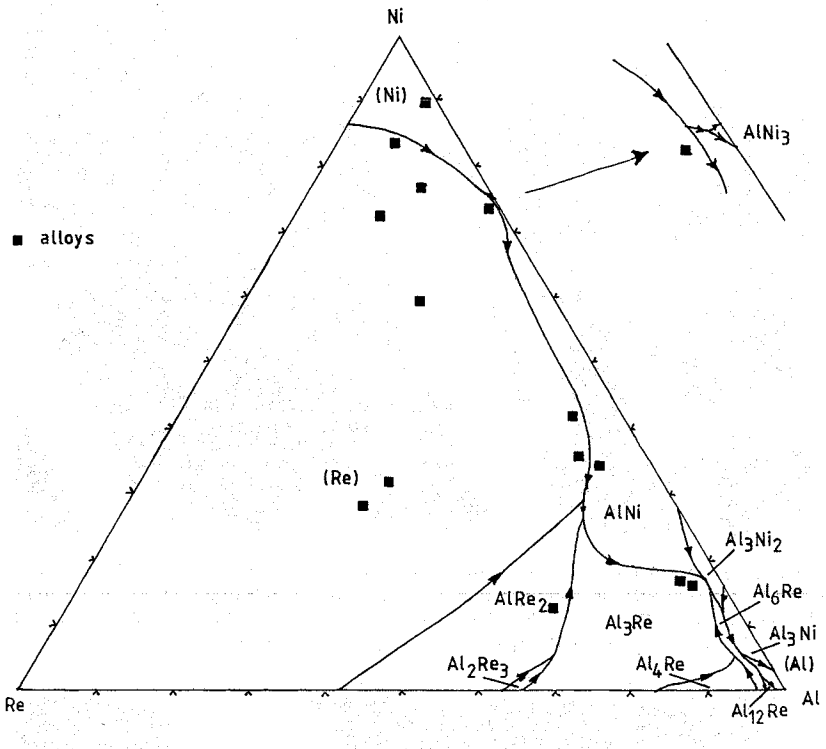

FIGURE 9 Liquidus surface for the Al–Ni–Re system (at.%).

the cooling sequence deduced from the microstructures. The phase field limits, invariant reaction compositions derived from the liquidus surface, and reaction temperatures will all be used as input for the Thermo-Calc system, to obtain assessed data.

SOME PITFALLS IN USING METALLOGRAPHY FOR REACTION ASSESSMENT

In the above case study, the importance of metallography as a valuable tool in phase equilibria deduction has been demonstrated. It can be used to identify the sequence of solidification, by finding the primary solidification phase: this has its own characteristic microstructure because being the first phase to form, it has complete spatial freedom, whereas subsequent phases have to fill in the remaining spaces. A good understanding of metallography can also be useful in unravelling the solidification sequence; for example in Figures 10 and 11 [34], the most likely sequence of solidification is (for the

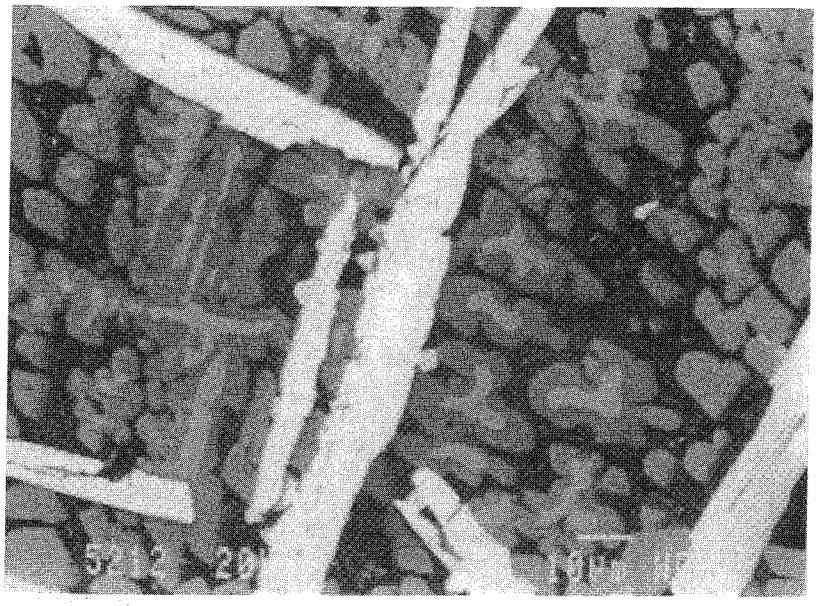

FIGURE 10 SEM image in backscattered electron mode. Al – 15 (at.%) Ni – 5 Re alloy illustrating the sequence of phase formation. In order of solidification: Al_3Re plates (lightest) with small, thick Al_6Re side-needles (light grey), Al_3Ni_2 inner dendrites (medium grey), Al_3Ni outer dendrites (dark grey), and Al_3Ni + (Al) (black) eutectic [34].

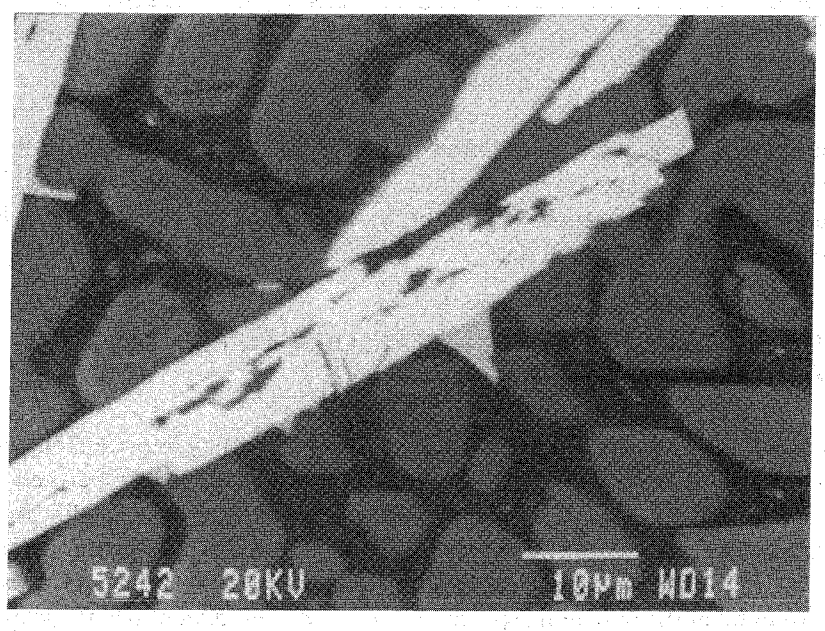

FIGURE 11 SEM image in backscattered electron mode. Al – 15 (at.%) Ni – 5 Re alloy showing the side-needless more clearly. Al_3Re plates (light) with small, thick Al_6Re side-needles (light grey), Al_3Ni dendrites (dark grey), and Al_3Ni + (Al) (black) eutectic [34].

ternary extensions of phases): primary Al_3Re (large plates), Al_6Re (smaller and thick needles on the large plates), Al_3Ni_2 (dendrite centres), Al_3Ni (dendrite outsides), and finally, the Al_3Ni + (Al) eutectic. This order was discerned by piecing together the two sub-sequences: firstly: plates, then the smaller and thick needles; with secondly: inner dendrites, then outer dendrites, and final eutectic reaction. An eutectic reaction is invariably the last reaction, because it is the only invariant reaction which lies at a local minimum of the liquidus. Careful study of the microstructure reveals the occasional contact of the inner dendrite with the smaller and thick needles on the plates (Fig. 11), although this does not always occur clearly, since the observed microstructure is only a section of the material.

Thus, metallography is an essential technique in phase equilibria studies, for deducing both the sequence of phases formed, and also their formation reactions. There have been at least two phase diagram studies in which eutectic reactions were missed, although the correct phases were identified, because metallography was not utilised [13, 33, 27, 35].

There are other examples where only metallography could discern the reaction type. The use of metallography allowed discovery of the transformation of the binary eutectic $L \rightarrow AlIr + Al_{2.7}Ir$ into peritectic reaction: L + (ternary) $AlIr \rightarrow$ (ternary) $Al_{2.7}Ir$ within the ternary Al–Ir–Ru system [27]. Although it was not the only method which was employed, metallography was the major technique used to deduce the position of the ternary invariant reaction: L + (Ir) → (Ru) + B2 in the Al–Ir–Ru system (with B2 being the continuous phase between AlIr and AlRu) [28]. The identification of the composition of the invariant reaction was achieved mainly because of the difference in morphologies in the two-phase structures on either side of the invariant reaction. X-ray diffraction was also used to confirm the structure of the second phase [28]. In the same study, metallography identified the L + $\sim Al_{53}Ir_{20}Ru_{27} \rightarrow$ (ternary) Al_2Ru + (ternary) $Al_{2.7}Ir$ reaction shown in Figure 12.

On the other hand, even if metallography is employed as a technique, there are still certain mistakes workers can make. Depending on the speed of solidification, especially if fast, and without subsequent annealing, a phase formed on solidification can be retained at lower temperatures, even if the phase diagram shows otherwise. An example of this phenomenon is the phase based on Fe_2Si found in commercial ferrosilicon [36]. In the binary Fe–Si system [21], this phase forms as part of an eutectic reaction, and subsequently decomposes at ~1040°C.

Difficulties in fully interpreting a cascade, or sequence, of peritectic reactions can occur, especially in binary systems. The fact that this does not

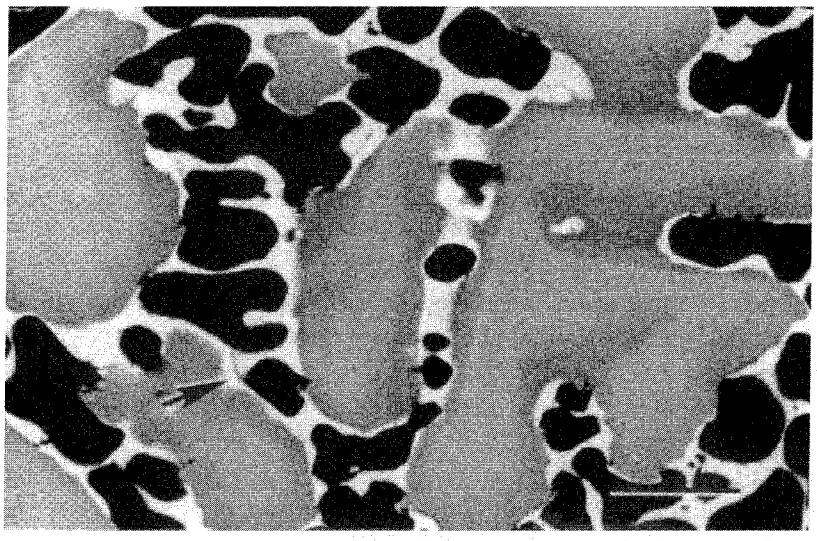

FIGURE 12 SEM image in backscattered electron mode. Al – 11 (at.%) Ir – 31 Ru alloy illustrating the L + $\sim Al_{53}Ir_{20}Ru_{27} \rightarrow Al_2Ru + Al_{2.7}Ir$ reaction. Previously-formed (cored) B2 dendrites (medium grey), rim of $\sim Al_{53}Ir_{20}Ru_{27}$ (light) (indicated by arrow), Al_2Ru (black) and $Al_{2.7}Ir$ (light grey) [28]. Bar represents 10 μm.

occur in higher order reactions is that there are more phases involved simultaneously, because there are more degrees of freedom (according to the phase rule), which usually makes identification easier. However, in binary systems, once again on fast cooling, where there is a cascade of peritectic reactions, the liquid composition can run a long way down the liquidus, so that none of the peritectic reactions actually achieves completion, and a layered structure results (Fig. 13) [37]. This is not so problematic in itself, except if the reaction temperatures are fairly close together, then a phase can either be skipped altogether, or formed, and subsequently consumed. Thus, different samples might give different phases. Consequently, the worker should use more than one sample in such regions, and then piece together the information.

Only as-solidified structures have been discussed so far. Once samples have been annealed, particularly if there is a transformation, then it can be difficult to deduce the actual nature of the transformation [38]. This is why, especially for an initial investigation, it is important to study as-solidified samples first, in order to identify the phases involved, and their reactions of formation. Another difficulty with peritectic phases, especially if the microstructure only comprises two phases, is to deduce which formed first.

FIGURE 13 SEM image in secondary electron mode. Al – 4 (at.%) Ru alloy showing the cascade of peritectic reactions, forming Al_3Ru_2, $Al_{13}Ru_4$ and Al_6Ru. From bottom left-hand corner: AlRu dendrites (lightest), Al_3Ru_2 dendrites (light grey), $Al_{13}Ru_4$ layer (medium grey), Al_6Ru (dark grey) with (Al) matrix (black) [37]. Bar represents 50 μm.

It is easy to recognise the interface between peritectic phases; it appears irregular because of the consumption of the solid parent phase to form the product. In a layered structure formed from multiple peritectic reactions, one simply works out from the centre (Fig. 13). However, where there are only two phases, one can often distinguish the product phase by searching for porosity, which is most likely associated with the last phase to solidify (Fig. 14) [27, 28, 39].

Coring can also be a problem. This phenomenon occurs when fast cooling does not allow sufficient diffusion to occur to equilibrate the compositional differences between the different layers deposited at lowering temperatures during solidification, when the phase diagram has a locally sloping liquidus and solidus. Usually the compositional difference between the cored layers is gradual, and a cored microstructure can be easily discerned from a true phase boundary. In Figure 15 [34], the lightest regions are one phase, whereas the other regions are a single cored phase. Occasionally, in a ternary or higher order system, there is a local steeper slope in the solidus, and the cored region appears to have a sharper boundary. A cored structure can be ascertained by undertaking a traverse of compositional analyses through the

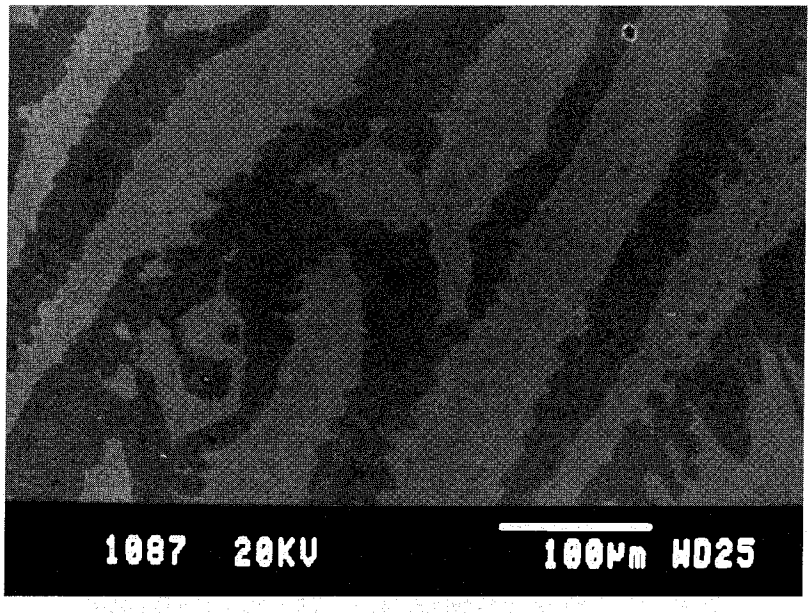

FIGURE 14 SEM image in backscattered electron mode. Al – 29 (at.%) Ir alloy demonstrating greater porosity associated with the product phase in the $L + Al_{2.7}Ir \rightarrow Al_3Ir$ peritectic reaction. Cored $Al_{2.7}Ir$ (light), Al_3Ir (medium grey) and porosity (black) [27, 28, 39].

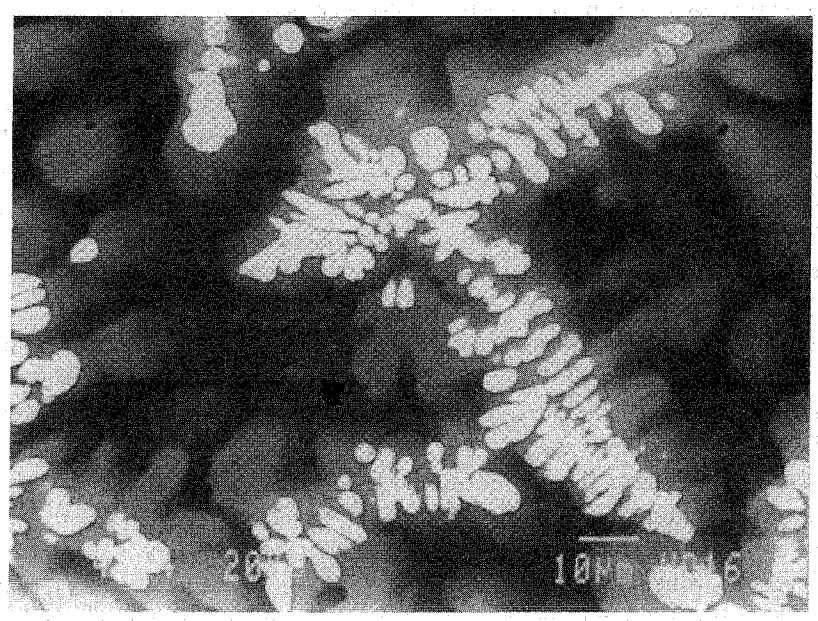

FIGURE 15 SEM image in backscattered electron mode. Al – 76 (at.%) Ni – 9 Re alloy showing the difference between coring and a separate phase. (Re) dendrites (light) with cored (Ni) (medium to dark grey) [34].

different components. An interface between two phases is indicated by a sharp change across the boundary, with only a small fluctuation, possibly caused by solute pile-up at a diffusion-controlled interface [40], whereas in coring, there will be a gradual change [41].

Sometimes a peritectic reaction can be wrongly deduced from a repressed eutectic reaction. If on (fast) cooling, after some pro-eutectic phase has solidified, the liquid composition overshoots the eutectic composition, the liquid becomes supersaturated with respect to the other phase which should be formed in the ensuing eutectic reaction. Thus, this phase is deposited first, and only once the liquid composition has returned to the eutectic composition, can the true eutectic reaction occur [42]. In Figure 16, a "halo" of metastable (ternary) AlNi formed around the primary (Re), and only once sufficient formation of this metastable phase had occurred, could the true stable (ternary) AlNi + (Re) eutectic form [34]. Care must be taken when studying these microstructures or else a peritectic reaction might be wrongly deduced. However, careful examination of the primary dendrites in Figure 16 reveals that they have a smooth outline, and so are not likely to have been partially consumed in a peritectic reaction.

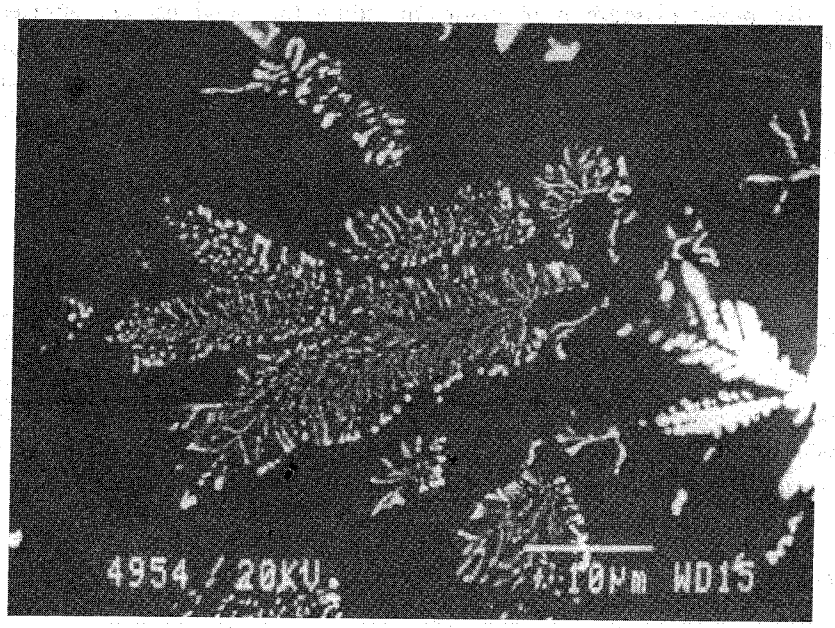

FIGURE 16 SEM image in backscattered electron mode. Al – 67 (at.%) Ni – 5 Re alloy illustrating the repressed L → (Re) + AlNi eutectic reaction. (Re) dendrites (light) surrounded by metastable AlNi matrix (dark), with (Re) + AlNi eutectic [34].

An additional incorrect deduction can be made due to the presence of porosity. If the porosity is subsurface and not identified as such, then a region of apparently lower average atomic number (*i.e.*, darker appearance) can be wrongly identified in backscattered electron mode in the SEM. The sometimes irregular appearance can even lead to a peritectic reaction being deemed responsible for the apparent phase. However, the check for this is to compare the average atomic numbers between the apparent phase and the surrounding matrix. A region with an underlying pore will not demonstrate the correct trend [27, 28].

CONCLUSIONS

A case study has been described in which metallography was a vital technique in interpreting the sequence of phases in the Al–Ni–Re system. Since published X-ray data were sparse, the spectra were identified with the aid of simulations based on input structural information, itself derived from a comparison of related phases and systems. Using metallography, EDS analyses and XRD measurements, recommendations for modifying the Al–Re phase diagram were made, including the previously unreported $Al_3Re + Al_2Re_3$ eutectic. The as-solidified phases in the Al–Ni–Re system, were identified and analysed, and a liquidus surface was produced. Additionally, typical pitfalls in the use of metallography were discussed and illustrated.

Acknowledgements

The authors thank the C.S.I.R (Mattek), the Microstructural Studies Research Programme at the University of the Witwatersrand, and the Foundation for Research and Development for financial support. In addition, R. Pennefather and C. M. Stander are thanked for their encouragement, while the contributions of P. J. Hill, T. D. Boniface, I. J. Horner, M. B. Cortie and Z. L. Nkosibomvu are acknowledged.

References

[1] Evans, D. S. and Prince, A. (1983). "The critical assessment of ternary alloy phase data", *J. Less Com. Met.*, **114**, 225.
[2] Ansara, I. (1979). "Comparison of methods for thermodynamic calculation of phase diagrams", *Int. Metal Reviews*, **1**, 20.

[3] Toop, G. W. (1965). "Predicting ternary activities using binary data", *Trans A.I.M.E*, **233**, 850.
[4] Kohler, F. (1960). *Montash. Chem.*, **91**, 738.
[5] Colinet, C. (1967). D.E.S., *Fac. Sci. Univ. Grenoble*, France.
[6] Muggianu, Y. M., Gambino, M. and Bros, J. P. (1975). *J. Chim. Phys.*, **72**(1), 83.
[7] Cornish, L. A. and Pratt, J. N. (1997). "Constitutional Studies of the Mo–Ru–Pd Ternary System", *J. Alloys and Compounds*, **247**, 66.
[8] Lukas, H. L., Henig, E. Th. and Zimmermann, B. (1977). "Optimisation of phase diagrams by a least squares method using simultaneously different types of data", *CALPHAD*, **1**(3), 225.
[9] JANAF Thermochemical Tables, Joint Army-Navy-Air Force Thermochemical Panel, Thermal Laboratory, Dow Chemical, Midland, MI (1967).
[10] Hultgren, R., Desai, P. D., Hawkins, D. T., Gleiser, M. and Kelley, K. K. (1973). Selected Values of the Thermodynamic Properties of the Elements and Alloys, American Society for Metals, Metals Park, OH.
[11] Thermo-Calc, The Thermo-Calc Group, Royal Institute of Technology, S 100 44 Stockholm, Sweden.
[12] Obrowski, W. (1960). "B2-phasen von Aluminium mit T-Metallen der VII. und VIII. Gruppe des Periodschen Systems", *Naturwissenschaften*, **47**, 14.
[13] Savitskii, E. M. (1961). *Russ. J. Inorg. Chem.*, **6**, 1003.
[14] Turkina, N. I. *et al.*, *Chemical Abstracts*, **79**, 8871m.
[15] Varich, A. N. *et al.*, *Metals Abstracts*, published by Inst. Metals and Am. Soc. Metals from 1968 onwards, **6**, 121230, 121231.
[16] d'Alte da Veiga, L. M. (1962). *Phil. Mag.*, **7**, 1247.
[17] Kripyakevich, P. I. and Kuzma, Yu. B. (1963). *Visn. Lvivsk. Derzh. Univ., Ser. Khim.*, **6**, 46.
[18] Minkevich, A. N., Tylinka, M. A., Rastorguev, L. N. and Rodionova, G. P. (1964). "Renii" (*Akad. Nauk SSSR, Inst. Met., Tr. 2-go [Vtorogo] Vses. Soveshch.*, 1962), p. 221, Izd, Nauka. Moscow.
[19] Schuster, J. C. (1984). "X-ray investigation of the phase relations and crystal structures in the binary system Re–Al", *J. Less Common Metals*, **98**, 215.
[20] Massalski, T. B., Ed. (1987). Binary Alloy Phase Diagrams, American Society of Metals, Ohio.
[21] Massalski, T. B., Ed.-in-chief (1990). (Eds.) Okamoto, H., Subramanian P. R. and Kacprzak L., Binary Alloy Phase Diagrams, 2nd edition, pub. William W. Scott Jnr.
[22] d'Alte da Veiga, L. M. (1962). " The aluminium–rhenium and aluminium–technetium systems: the new phases $ReAl_6$ and $TcAl_6$", *Phil. Mag.*, **7**, 193.
[23] d'Alte da Veiga, L. M. (1963). "The phase diagrams of the aluminium–rhenium and aluminium–technetium systems", *Phil. Mag.*, **8**, 1241.
[24] Wilkinson, C. (1967). "The refinement of the structures of the intermetallic phases $ReAl_6$ and $TcAl_6$", *Acta Cryst.*, **22**, 924.
[25] Magnéli, A., Edshammer, L. and Dagerhamn, T. (1962). Final Technical Report 1, on contract DA-91-591-EUC-2734 (AD 426927) p. 43.
[26] Kripyakevich, P. I. and Kuzma, Yu. B. (1962). *Kristallografiya*, **7**, 309; *Translation*: *Soviet Phys. Cryst.*, **7**, 240.
[27] Hill, P., Cornish, L. A. and Witcomb, M. J., "Modifications to the Al–Ir Phase Diagram", *Proc. Microsc. Soc. South. Afr.*, Vol. 27, p. 17, Bellville, December 1997.
[28] Hill, P., Cornish, L. A. and Witcomb, M. J., "Constitution of the Al–Ir–Ru system", submitted to *J. Alloys and Compounds.*
[29] Villars, P. and Calvert, L. D. (1985). Pearson's Handbook of Crystallographic Data for Intermetallic Phases, *Amer. Soc. Metals*, Ohio 44073.
[30] CC Miller program by C.L. Churms, National Accelerator Centre, P.O. Box.72, Faure, 7131 S. Africa.
[31] JCPDS-ICCD, Newtown Square, PA 19073, USA (1995).
[32] Cornish, L. A. and Witcomb, M. J., "Solidification Microstructures of some Al–Re Alloys", *Proc. Microsc. Soc. South. Afr.*, Vol. 27, p. 15, Bellville, December 1997.
[33] Cornish, L. A., "A study of the Ni–Al–Re system with nickel contents above ~60 atomic %, Part 1: An evaluation of the Al–Re binary system". Report to Mattek, C.S.I.R, Pretoria (September 1997).

[34] Cornish, L. A. (1998). "A Study of the Ni–Al–Re System with Nickel contents above ~60 atomic %, Part 2: Experimental Evaluation of the Al–Re Binary System and the Al–Ni–Re Ternary System", Report to Mattek, C.S.I.R, Pretoria (February 1998).
[35] Axler, K. M., Foltyn, E. M., Peterson, D. E. and Hutchinson, W. B. (1989). "Phase investigations of the Al–Ir system", *J. Less Common Metals*, **156**, 213.
[36] Nkosibomvu, Z. L., Witcomb, M. J., Cornish, L. A. and Pollak, H. (1998). "Mössbauer Spectroscopy and SEM Characterisation of Commercial Ferrosilicon Powders", *Hyperfine Interactions*, **112**, 261.
[37] Boniface, T. D. and Cornish, L. A. (1996). "An Investigation of the High Aluminium end of the Al–Ru Phase diagram", *J. Alloys and Compounds*, **233**, 241.
[38] Cornish, L. A. (1986). "Computer Calculation of Phase Diagrams including the Molybdenum-Based Intermetallics in Uranium Dioxide Fuel Pins", *Ph.D. Thesis*, University of Birmingham, UK.
[39] Hill, P. J., Cornish, L. A. and Witcomb, M. J. (1998). "Constitution and Hardnesses of the Al–Ir System", *J. Alloys and Compounds*, **280**, 240.
[40] Jackson, E. M. L. E. M. (1997). "Kinetics of Sigma Formation and Dissolution in Duplex Stainless Steels". *Ph.D. Thesis*, University of the Witwatersrand, Johannesburg.
[41] Horner, I. J., Hall, N., Cornish, L. A., Witcomb, M. J., Cortie, M. B. and Boniface, T. D. (1998). "An Investigation of the B2 Phase between AlRu and AlNi in the Al–Ni–Ru Ternary System", *J. Alloys and Compounds*, **264**, 173.
[42] Gigliotti, M. F. X., Colligan, G. A. and Powell, G. F. (1970). *Met. Trans. A.I.M.E.*, **1**, 2046.